Exciton topology and condensation in a model quantum spin Hall insulator

Andrea Blason and Michele Fabrizio

International School for Advanced Studies (SISSA), Via Bonomea 265, I-34136 Trieste, Italy

We study by a consistent mean-field scheme the role on the single- and two-particle properties of a local electron-electron repulsion in the Bernevig, Hughes, and Zhang model of a quantum spin Hall insulator. We find that the interaction fosters the intrusion between the topological and nontopological insulators of an insulating and magnetoelectric phase that breaks spontaneously inversion and time-reversal symmetries but not their product. The approach to this phase from both topological and nontopological sides is signaled by the softening of two exciton branches, i.e., whose binding energy reaches the gap value, that possess, in most cases, finite and opposite Chern numbers, thus allowing this phase to be regarded as a condensate of topological excitons. We also discuss how those excitons, and especially their surface counterparts, may influence the physical observables.

I. INTRODUCTION

The physics of excitons in topological insulators has attracted considerable interest in the last decade, see, not as an exhaustive list, Refs. [1–8], recently renewed [9] by the evidence of a quantum spin Hall effect in two-dimensional transition-metal dichalcogenides [10–12]. More precisely, a consistent part of the research activity has focused on the possibility of an exciton condensation in thin samples of topological insulators [1–3,7,13–15], much in the spirit of what was proposed [16,17] and observed [18] in bilayer graphene. In addition, the puzzling properties of the purported topological Kondo insulator SmB_6 [19–21] prompted interest in the excitons of such material [4–6,22–24] as partly responsible for its anomalous behavior.

Even though evidence of excitons also exists in the three-dimensional topological insulator Bi_2Se_3 [8], besides those in the still controversial SmB_6, a systematic study in model topological insulators is largely lacking [22,25–27]. Our aim here is to partly fill this gap. Specifically, we consider the prototypical model of a quantum spin Hall insulator (QSHI) introduced by Bernevig, Hughes, and Zhang (BHZ) [28], and add a local interaction compatible with the symmetries, which, e.g., allow for a dipole-dipole term. We deal with such an interaction in a conserving mean-field scheme. Namely, we assume the Hartree-Fock (HF) expression of the self-energy functional to compute the single-particle Green's function. Next, we calculate the excitons by solving the Bethe-Salpeter equations for the response functions, using as an irreducible vertex the functional derivative of the HF self-energy functional with respect to the Green's function; what is often called random phase approximation plus exchange [29].

Our main result is that, starting from the noninteracting QSHI, branches of excitons that transform into each other under time reversal detach from the continuum of particle-hole excitations and gradually soften upon increasing interaction strength. When the latter exceeds a critical value, those excitons become massless and thus condense through a second-order critical point, which coincides with that obtained directly through the HF calculation not forcing any symmetry. Such a symmetry-broken phase is still insulating and displays magnetoelectric effects. Upon further increasing interaction, it eventually gives in to the nontopological symmetry invariant insulator via another second-order transition. None of those transitions is accompanied by any gap closing; therefore, uncovering a path between the QSHI and the trivial insulator that does not cross any gapless point [30–32], thanks to the interaction-driven spontaneous breakdown of time reversal symmetry.

We also find that, approaching the excitonic insulator from the QSHI, the excitons themselves may acquire a nontrivial topology signaled by a nonzero Chern number, suggestive of the existence of chiral exciton edge modes. In addition, we have evidence that, in open boundary geometries, exciton condensation occurs at the surface earlier than in the bulk, which also foresees the existence of nonchiral surface excitons that go soft before the bulk ones [33–35].

Our findings may have observable consequences that we discuss, some of which are not in disagreement with existing experimental evidence.

This work is organized as follows. In Sec. II, we introduce the interacting model Hamiltonian, while the conserving HF approximation that we use to deal with interaction is discussed in Secs. III and IV. The results of the calculations are presented in Sec. V; specifically, in Sec. V A, the HF phase diagram; in Sec. V B the excitons in the QSHI phase; and, finally, in Sec. V C the magnetoelectric effect in the excitonic insulator. Section VI is devoted to concluding remarks.

II. THE MODEL HAMILTONIAN

We shall consider the BHZ model, introduced to describe the QSHI phase in HgTe quantum wells [28]. The BHZ model involves two spinful Wannier orbitals per unit cell, which transform like s orbitals, $|s\sigma\rangle$, where $\sigma = \uparrow, \downarrow$ refers to the projection of the spin along the z axis, and like the $J = 3/2$,

$J_z = \pm 3/2$ spin-orbit coupled combinations of p orbitals, i.e.,

$$|p_x + i p_y \uparrow\rangle = |p_{+1} \uparrow\rangle \equiv |p \uparrow\rangle \,,$$
$$|p_x - i p_y \downarrow\rangle = |p_{-1} \downarrow\rangle \equiv |p \downarrow\rangle \,. \tag{1}$$

We introduce two sets of Pauli matrices, σ_a and τ_a, $a = 0, \dots, 3$, with $a = 0$ denoting the identity, which act, respectively, in the spin, $\uparrow$ and $\downarrow$, and orbital, s and p, spaces.

With those definitions, the BHZ tight-binding Hamiltonian on a square lattice includes all on-site potentials and nearest-neighbor hopping terms that are compatible with inversion, time reversal, and C_4 symmetry [36], and reads

$$\mathcal{H}_0 = \sum_{\mathbf{k}} \boldsymbol{\Psi}_{\mathbf{k}}^\dagger \, \hat{H}_0(\mathbf{k}) \, \boldsymbol{\Psi}_{\mathbf{k}} = \sum_{ij} \boldsymbol{\Psi}_i^\dagger \, \hat{H}_0(\mathbf{R}_i - \mathbf{R}_j) \, \boldsymbol{\Psi}_j, \tag{2}$$

at density corresponding to two electrons per site, where

$$\boldsymbol{\Psi}_{\mathbf{k}} = \begin{pmatrix} s_{\mathbf{k}\uparrow} \\ s_{\mathbf{k}\downarrow} \\ p_{\mathbf{k}\uparrow} \\ p_{\mathbf{k}\downarrow} \end{pmatrix}, \quad \boldsymbol{\Psi}_i = \begin{pmatrix} s_{i\uparrow} \\ s_{i\downarrow} \\ p_{i\uparrow} \\ p_{i\downarrow} \end{pmatrix}, \tag{3}$$

are four component spinors in momentum, $\boldsymbol{\Psi}_{\mathbf{k}}$, and real, $\boldsymbol{\Psi}_i$, space, with i labeling the unit cell at position $\mathbf{R}_i$. $\hat{H}_0(\mathbf{k})$ is the 4×4 matrix

$$\hat{H}_0(\mathbf{k}) = (M - t\,\epsilon_{\mathbf{k}})\,\sigma_0 \otimes \tau_3 - t'\,\epsilon_{\mathbf{k}}\,\sigma_0 \otimes \tau_0$$
$$+ \lambda \sin k_x\, \sigma_3 \otimes \tau_1 - \lambda \sin k_y\, \sigma_0 \otimes \tau_2 \,, \tag{4}$$

with $\mathbf{k} = (k_x, k_y)$ and $\epsilon_{\mathbf{k}} = (\cos k_x + \cos k_y)$ while $\hat{H}_0(\mathbf{R}_i - \mathbf{R}_j)$ is its Fourier transform in real space. The parameters $t' - t$, $t' + t$, and λ correspond, respectively, to the $s - s$, $p - p$, and $s - p$ nearest-neighbor hybridization amplitudes. Finally, M describes an on-site energy difference between the two orbitals.

Hereafter, we shall analyze the Hamiltonian Eq. (4) for $M > 0$, $t' = 0.5\,t$, and $\lambda = 0.3\,t$. The precise values of the latter two are not crucial to the physics of the model. What really matters is the relative magnitude of M and t and the finiteness of λ. Therefore, for the sake of simplicity, we shall set $t = 1$ as the unit of energy.

The band structure can be easily calculated and yields two bands, each degenerate with respect to the spin label σ; a conduction and a valence band, with dispersion $\epsilon_c(\mathbf{k})$ and $\epsilon_v(\mathbf{k})$, respectively, which read

$$\epsilon_c(\mathbf{k}) = -t'\,\epsilon_{\mathbf{k}} + E_{\mathbf{k}}, \quad \epsilon_v(\mathbf{k}) = -t'\,\epsilon_{\mathbf{k}} - E_{\mathbf{k}}, \tag{5}$$

where

$$E_{\mathbf{k}} = \sqrt{(M - \epsilon_{\mathbf{k}})^2 + \lambda^2 \sin^2 k_x + \lambda^2 \sin^2 k_y} \,. \tag{6}$$

With our choice of parameters, these bands describe a direct gap semiconductor for any $M \neq 2$. At the high-symmetry points in the Brillouin zone (BZ), the bands have a defined orbital character, i.e., a defined parity under inversion. Specifically, at $\boldsymbol{\Gamma} = (0, 0)$,

$$\epsilon_c(\boldsymbol{\Gamma}) = -2t' + |M - 2|, \quad \epsilon_v(\boldsymbol{\Gamma}) = -2t' - |M - 2|, \tag{7}$$

valence and conduction bands have, respectively, s and p orbital character if $M < 2$, and vice versa if $M > 2$. On
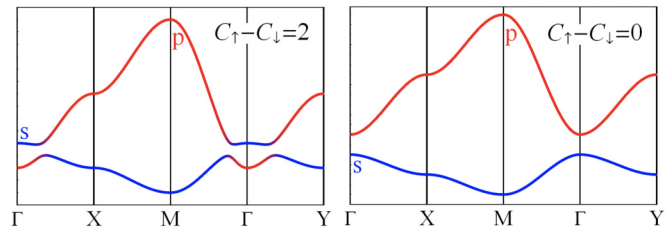

FIG. 1. Band structure of the BHZ model in the topological (left panel) and trivial (right panel) regimes. Blue and red colors indicate, respectively, even (s orbital character) and odd (p orbital character) parity under inversion.

the contrary, at the zone boundary points $\boldsymbol{M} = (\pi, \pi)$, $\boldsymbol{X} = (\pi, 0)$, and $\boldsymbol{Y} = (0, \pi)$,

$$\begin{aligned} \epsilon_c(\boldsymbol{M}) &= 2t' + (M + 2), \quad \epsilon_v(\boldsymbol{M}) = 2t' - (M + 2), \\ \epsilon_c(\boldsymbol{X}) &= \epsilon_c(\boldsymbol{Y}) = M, \quad \epsilon_v(\boldsymbol{X}) = \epsilon_v(\boldsymbol{Y}) = -M, \end{aligned} \tag{8}$$

the valence band is p and the conduction s for any value of M. It follows that, if $M < 2$, there is an avoided band crossing, due to $\lambda \neq 0$, moving from $\boldsymbol{\Gamma}$ toward the BZ boundary, while, if $M > 2$, each band has predominantly a single orbital character, s the conduction band, and p the valence one, see Fig. 1. At $M = 2$, the gap closes at $\boldsymbol{\Gamma}$, around which the dispersion becomes Dirac-like:

$$\epsilon_c(\mathbf{k}) \simeq +\lambda\,|\mathbf{k}|, \quad \epsilon_v(\mathbf{k}) \simeq -\lambda\,|\mathbf{k}|. \tag{9}$$

The transition between the two insulating phases is known to have topological character [28].

We note that the Hamiltonian $\hat{H}_0(\mathbf{k})$ commutes with σ_3, i.e., is invariant under $U(1)$ spin rotations around the z axis, as well as under inversion and time reversal, respectively, represented by the operators

$$\begin{aligned} \mathcal{I} &: \hat{H}_0(\mathbf{k}) = \sigma_0 \otimes \tau_3 \, \hat{H}_0(-\mathbf{k}) \, \sigma_0 \otimes \tau_3 \,, \\ \mathcal{T} &: \hat{H}_0(\mathbf{k}) = (-i\sigma_2 \otimes \tau_0) \, \hat{H}_0^*(-\mathbf{k}) \, (i\sigma_2 \otimes \tau_0). \end{aligned} \tag{10}$$

In addition, it is invariant under spatial, i.e., not affecting spins, C_4 rotations, which correspond to

$$\mathcal{C}_4 : \hat{H}_0(\mathbf{k}) = e^{-i\frac{\pi}{2} L_3} \, \hat{H}_0(C_4(\mathbf{k})) \, e^{i\frac{\pi}{2} L_3}, \tag{11}$$

where $C_4(\mathbf{k}) = (k_y, -k_x)$, and the z component of the angular momentum operator is

$$L_3 = \sigma_3 \otimes \frac{\tau_0 - \tau_3}{2} \,. \tag{12}$$

Evidently, since the Hamiltonian is also invariant under spin $U(1)$ rotations, with generator $S_3 = \sigma_3 \otimes \tau_0/2$, it is also invariant under $\pi/2$ rotations with generator the total angular momentum along z, i.e., $J_3 = L_3 + S_3$, which provides a better definition of C_4.

We observe that, if C_σ is the Chern number of the spin-σ valence-band electrons, then invariance under both inversion and time reversal entails a vanishing $(C_\uparrow + C_\downarrow)$, which is proportional to the transverse charge conductance, but a possibly nonzero $(C_\uparrow - C_\downarrow)$, which would correspond to a finite transverse spin-conductance, thus the nontrivial topology of a QSHI [37]. Specifically, $(C_\uparrow - C_\downarrow) \neq 0$ occurs when $M < 2$ [28,30], not surprisingly in view of the avoided band

crossings. We emphasize that a robust topological invariant can be defined provided spin $U(1)$ symmetry is preserved.

So far, we have discussed the main properties of the noninteracting Hamiltonian Eq. (2). However, physically, electrons unavoidably interact with each other. We shall therefore add to the noninteracting Hamiltonian Eq. (2) a local Coulomb interaction U_{int}, thus neglecting its long-range tail, which includes, besides monopoles terms, also a dipole-dipole interaction U_{dip}, which is here allowed by symmetry. Specifically,

$$U_{\text{int}} = U + U_{\text{dip}}, \tag{13}$$

where

$$U = \sum_i (U_s\, n_{is\uparrow} n_{is\downarrow} + U_p\, n_{ip\uparrow} n_{ip\downarrow} + V\, n_{is} n_{ip}) \tag{14}$$

includes monopole terms, while the dipole-dipole interaction, projected onto our basis of single-particle wave functions, reads

$$U_{\text{dip}} = \frac{J}{2} \sum_i [(\boldsymbol{\Psi}_i^\dagger\, \sigma_0 \otimes \tau_1\, \boldsymbol{\Psi}_i)^2 + (\boldsymbol{\Psi}_i^\dagger\, \sigma_3 \otimes \tau_2\, \boldsymbol{\Psi}_i)^2]. \tag{15}$$

All coupling constants, U_s, U_p, V, and J, are positive, $n_{is\sigma} = s_{i\sigma}^\dagger s_{i\sigma}$, $n_{ip\sigma} = p_{i\sigma}^\dagger p_{i\sigma}$, and $n_{is(p)} = n_{is(p)\uparrow} + n_{is(p)\downarrow}$. Hereafter, to reduce the number of independent parameters and thus simplify the analysis, we shall take $U_s = U_p = U$. Moreover, the numerical solution will be carried out with the further simplification $U = V$.

We end mentioning that a calculation similar to the one we are going to present has already been performed by Chen and Shindou [26], though in the magnetized BHZ model, which includes just two orbitals, $|s \uparrow\rangle$ and, different from our time-reversal invariant case, see Eqs. (1), the $J = 3/2$, $J_z = +1/2$ orbital $|p_{+1} \downarrow\rangle$.

III. HARTREE-FOCK APPROXIMATION

The simplest way to include the effects of a not-too-strong interaction is through the HF approximation, which amounts to approximating the self-energy functional simply by the HF diagrams. For sake of simplicity, we shall introduce the HF approximation under the assumption of unbroken translational symmetry, so the lattice total momentum is a good quantum number. Whenever needed, we will mention what changes when translational symmetry is broken.

Within the HF approximation, if

$$\hat{G}_0(i\epsilon, \mathbf{k})^{-1} = i\epsilon - \hat{H}_0(\mathbf{k}) \tag{16}$$

is the inverse of the noninteracting 4×4 Green's function matrix at momentum $\mathbf{k}$ and in Matsubara frequencies, $i\epsilon$, the interacting Green's function is

$$\hat{G}(i\epsilon, \mathbf{k})^{-1} = \hat{G}_0(i\epsilon, \mathbf{k})^{-1} - \hat{\Sigma}_{\text{HF}}[\hat{G}], \tag{17}$$

where, in the specific case under consideration, the self-energy within the HF approximation is functional of the local

Green's function,

$$\hat{\Sigma}_{\text{HF}}[\hat{G}(\mathbf{R}_i, \mathbf{R}_i)] = \sum_{\alpha, a=0}^3 \sigma_\alpha \otimes \tau_a\, \Gamma_{\alpha a}^0\, \Delta_{\alpha a}(\mathbf{R}_i), \tag{18}$$

with

$$\Delta_{\alpha a}(\mathbf{R}_i) \equiv T \sum_\epsilon e^{i\epsilon\, 0^+}\, \text{Tr}(\hat{G}(i\epsilon, \mathbf{R}_i, \mathbf{R}_i)\, \sigma_\alpha \otimes \tau_a)$$

$$= \langle \boldsymbol{\Psi}_i^\dagger\, \sigma_\alpha \otimes \tau_a\, \boldsymbol{\Psi}_i \rangle \equiv \langle \text{O}_{\alpha a}(\mathbf{R}_i) \rangle \in \mathbb{R}, \tag{19}$$

which become independent of the site coordinates $\mathbf{R}_i$ if translational symmetry holds, i.e., $\Delta_{\alpha a}(\mathbf{R}_i) \to \Delta_{\alpha a}$, $\forall \mathbf{R}_i$. The Dyson Eq. (17), together with Eqs. (18) and (19), yield a self-consistency condition that has to be solved. $\Gamma_{\alpha a}^0$ are the irreducible scattering amplitudes in the HF approximation and, through Eq. (13), their expressions can be readily derived:

$$\Gamma_{00}^0 = \frac{U + 2V - 2J}{4}, \quad \Gamma_{03}^0 = \frac{U - 2V + 2J}{4},$$

$$\Gamma_{01}^0 = -\frac{V - 4J}{4}, \quad \Gamma_{02}^0 = -\frac{V}{4},$$

$$\Gamma_{10}^0 = \Gamma_{20}^0 = -\frac{U}{4}, \quad \Gamma_{30}^0 = -\frac{U + 2J}{4},$$

$$\Gamma_{11}^0 = \Gamma_{21}^0 = -\frac{V + 2J}{4}, \quad \Gamma_{31}^0 = -\frac{V}{4},$$

$$\Gamma_{12}^0 = \Gamma_{22}^0 = -\frac{V - 2J}{4}, \quad \Gamma_{32}^0 = -\frac{V - 4J}{4},$$

$$\Gamma_{13}^0 = \Gamma_{23}^0 = -\frac{U}{4}, \quad \Gamma_{33}^0 = -\frac{U - 2J}{4}. \tag{20}$$

We note that the scattering amplitudes posses the same spin $U(1)$ symmetry of the noninteracting Hamiltonian, namely, $\Gamma_{1a}^0 = \Gamma_{2a}^0 \neq \Gamma_{3a}^0$, $a = 0, \ldots, 3$.

The expectation values $\Delta_{00}(\mathbf{R}_i) = \langle n_{is} + n_{ip} \rangle$ and $\Delta_{03}(\mathbf{R}_i) = \langle n_{is} - n_{ip} \rangle$, which measure the local density and orbital polarization, respectively, are finite already in absence of interaction. In this case, the effects of the scattering amplitudes Γ_{00}^0 and Γ_{03}^0 treated within HF are, respectively, to shift the chemical potential, which we can discard since we work at fixed density, and renormalise upward the value of M, thus enlarging the stability region of the nontopological phase.

On the contrary, all other expectation values $\Delta_{\alpha a}(\mathbf{R}_i)$, $(\alpha, a) \neq (0, 0), (0, 3)$, break one or more symmetries of the noninteracting Hamiltonian and therefore vanish identically in the noninteracting case. They could become finite should interaction be strong enough to lead to spontaneous symmetry breaking. We expect this should primarily occur in those channels whose scattering amplitudes are the most negative ones, being $\Delta_{\alpha a}(\mathbf{R}_i)$ real by definition. If $V \simeq U$, as we shall assume in the following numerical calculations, the dominant symmetry-breaking channels are therefore those with $(\alpha, a) = (3, 0), (1, 1), (2, 1)$. We emphasize that the dipolar coupling constant J plays an important role in splitting the large degeneracies of the scattering amplitudes in Eqs. (20) that exist at $J = 0$.

Specifically,

$$\Delta_{30}(\mathbf{R}_i) = \langle \boldsymbol{\Psi}_i^\dagger\, \sigma_3 \otimes \tau_0\, \boldsymbol{\Psi}_i \rangle = \sum_{l=s,p} \langle n_{il\uparrow} - n_{il\downarrow} \rangle \tag{21}$$

corresponds to a spontaneous spin polarization along the z axis, which breaks time-reversal symmetry. We shall investigate two possible magnetic orders, $\Delta_{30}(\mathbf{R}_i) = \Delta_{30}\, e^{i\mathbf{Q}\cdot\mathbf{R}_i}$, with $\mathbf{Q} = (0,0)$ or $\mathbf{Q} = (\pi,\pi)$, corresponding, respectively, to ferromagnetism or antiferromagnetism. We point out that the latter implies a breakdown of translational symmetry, in which case the Green's function is not diagonal anymore in $\mathbf{k}$, but depends on it as well as on $\mathbf{k}+\mathbf{Q}$, so it becomes an 8×8 matrix and Eq. (17) must be modified accordingly.

On the contrary,

$$
\begin{aligned}
\Delta_{11}(\mathbf{R}_i) &= \langle \mathbf{\Psi}_i^\dagger\, \sigma_1 \otimes \tau_1\, \mathbf{\Psi}_i \rangle \\
&= \sum_{\sigma=\uparrow,\downarrow} \langle s_{i\sigma}^\dagger\, p_{i-\sigma} + p_{i\sigma}^\dagger\, s_{i-\sigma} \rangle,
\end{aligned}
$$

$$
\begin{aligned}
\Delta_{21}(\mathbf{R}_i) &= \langle \mathbf{\Psi}_i^\dagger\, \sigma_2 \otimes \tau_1\, \mathbf{\Psi}_i \rangle \\
&= -i \sum_{\sigma=\uparrow,\downarrow} \sigma\, \langle s_{i\sigma}^\dagger\, p_{i-\sigma} + p_{i\sigma}^\dagger\, s_{i-\sigma} \rangle, \quad (22)
\end{aligned}
$$

describe a spin-triplet exciton condensate polarized in the plane. Since the insulator has a direct gap, excitons condense at $\mathbf{Q} = 0$, namely, $\Delta_{\alpha 1}(\mathbf{R}) = \Delta_{\alpha 1}$, $\forall\, \mathbf{R}$, and $\alpha = 1, 2$. Moreover, because $\Gamma_{11}^0 = \Gamma_{21}^0$, if we write

$$
\Delta_{11} = \Delta \cos\phi, \quad \Delta_{21} = \Delta \sin\phi, \quad (23)
$$

we expect to find a solution with the same amplitude Δ for any value of ϕ, which reflects the spin $U(1)$ symmetry. At any given ϕ, such exciton condensation would break spin $U(1)$, inversion, and time-reversal symmetry.

The emergence of an exciton condensate is therefore accompanied by a spontaneous spin $U(1)$ symmetry breaking. As previously mentioned, such breakdown prevents the existence of the strong topological invariant that characterizes the QSHI phase. Specifically, since the z component of the spin is not a good quantum number anymore, the counterpropagating edge states of opposite spin are allowed to couple each other, which turns their crossing into an avoided one [30]. The boundary thus becomes insulating, spoiling the topological transport properties of the QSHI.

We shall study this phenomenon performing an HF calculation in a ribbon geometry with open boundary conditions (OBCs) along x, but periodic ones along y. Consequently, the noninteracting BHZ Hamiltonian loses translational invariance along the x direction, while keeping it along y, so the Green's function becomes a $4N_x \times 4N_x$ matrix for each momentum k_y, with N_x the number of sites along x. A further complication is that HF self-energy in Eq. (17) unavoidably depends on the x coordinate of each site, which enlarges the number of self-consistency equations to be fulfilled. However, since those equations can be easily solved iteratively, we can still numerically afford ribbon widths, i.e., values of N_x, which provide physically sensible results with negligible size effects.

The OBC calculation gives access not only to the states that may form at the boundaries, but also, in the event of a spontaneous symmetry breaking, to the behavior of the corresponding order parameter moving from the edges toward the bulk interior. In practice, we shall investigate such circumstance only in the region of Hamiltonian parameters when the dominant instability is toward the spin-triplet exciton condensation.

IV. BETHE-SALPETER EQUATION

If we start from the QSHI, $M < 2$, and adiabatically switch on the interaction Eq. (13), we expect that such a phase will for a while survive because of the gap, until, for strong enough interaction, it will eventually give up to a different phase. We already mentioned that the first effect of interaction is to renormalize upward M, thus pushing the topological insulator toward the transition into the nontopological one. In addition, a repulsive interaction can also bind across gap particle-hole excitations, i.e., create excitons.

A direct way to reveal excitons is through the in-gap poles of linear response functions. Within the HF approximation for the self-energy functional, the linear response functions must be calculated, solving the corresponding Bethe-Salpeter (BS) equations using the HF Green's functions together with the irreducible scattering amplitudes in Eqs. (20), which are actually the functional derivatives of $\hat{\Sigma}_{\mathrm{HF}}[\hat{G}]$ with respect to $\hat{G}$.

If the interaction is indeed able to stabilize in-gap excitons, their binding energy must increase with increasing interaction strength. It is therefore very possible that the excitons touch zero energy at a critical interaction strength, which would signal an instability toward a different, possibly symmetry-variant phase. Consistency of our approximation requires that such instability should also appear in the unconstrained HF calculation as a transition from the topological insulator to another phase, especially if such transition were continuous. We shall check that is indeed the case.

With our notations, see Eqs. (19) and (20), a generic correlation function will be defined as

$$
\chi_{\alpha a;\beta b}(\tau, \mathbf{R}) \equiv -\langle T_\tau\big(O_{\alpha a}(\tau, \mathbf{R})\, O_{\beta b}(0, \mathbf{0})\big)\rangle, \quad (24)
$$

where T_τ is the time-ordering operator and the operators $O_{\alpha a}(\mathbf{R}_i) = \mathbf{\Psi}_i^\dagger \sigma_\alpha \otimes \tau_a \mathbf{\Psi}_i$ are evolved in imaginary time τ. Spin $U(1)$ symmetry implies that the z-component S_z of the total spin is conserved. It follows that the only nonzero correlation functions $\chi_{\alpha a;\beta b}$ have α and β either 0 and 3, corresponding to $S_z = 0$, or 1 and 2, satisfying

$$
\begin{aligned}
\chi_{1a;1b}(\tau, \mathbf{R}) &= \chi_{2a;2b}(\tau, \mathbf{R}), \\
\chi_{1a;2b}(\tau, \mathbf{R}) &= -\chi_{2a;1b}(\tau, \mathbf{R}), \quad (25)
\end{aligned}
$$

whose combinations $\chi_{1a;1b} \pm i\,\chi_{1a;2b}$ describe the independent propagation of $S_z = \pm 1$ particle-hole excitations.

The Fourier transform $\chi_{\alpha a;\beta b}(i\omega, \mathbf{q})$, in momentum and in Matsubara frequencies, are obtained through the solution of a set of BS equations,

$$
\begin{aligned}
\chi_{\alpha a;\beta b}(i\omega, \mathbf{q}) &= \chi_{\alpha a;\beta b}^{(0)}(i\omega, \mathbf{q}) + \sum_{\gamma c} \chi_{\alpha a;\gamma c}^{(0)}(i\omega, \mathbf{q})\, \Gamma_{\gamma c}^0 \\
&\quad \times \chi_{\gamma c;\beta b}(i\omega, \mathbf{q}), \quad (26)
\end{aligned}
$$

where

$$
\begin{aligned}
\chi_{\alpha a;\beta b}^{(0)}(i\omega, \mathbf{q}) &= \frac{1}{N}\sum_{\mathbf{k}} T \sum_\epsilon \mathrm{Tr}\big(\sigma_\alpha \otimes \tau_a \\
&\quad \times \hat{G}(i\epsilon + i\omega, \mathbf{k}+\mathbf{q})\, \sigma_\beta \otimes \tau_b\, \hat{G}(i\epsilon, \mathbf{k})\big). \quad (27)
\end{aligned}
$$

In Eq. (27), N is the number of sites and $\hat{G}(i\epsilon, \mathbf{k})$ the HF Green's function matrices.

We shall perform the above calculation at zero temperature without allowing in the HF calculation any symmetry breaking. With this assumption, the HF Green's function reads

$$\hat{G}(i\epsilon, \mathbf{k}) = \frac{(i\epsilon + t'\epsilon_{\mathbf{k}}) \, \sigma_0 \otimes \tau_0 + \hat{H}_{\mathrm{HF}}(\mathbf{k})}{(i\epsilon - \epsilon_c(\mathbf{k}))(i\epsilon - \epsilon_v(\mathbf{k}))}, \qquad (28)$$

where $\hat{H}_{\mathrm{HF}}(\mathbf{k})$, $\epsilon_c(\mathbf{k})$, and $\epsilon_v(\mathbf{k})$ are those in Eqs. (4) and (5), with M in Eqs. (4) and (6) replaced by an effective M_{HF} determined through the self-consistency equation:

$$M_{\mathrm{HF}} = M - \frac{2\,\Gamma_{03}^0}{N} \sum_{\mathbf{k}} \frac{M_{\mathrm{HF}} - \epsilon_{\mathbf{k}}}{E_{\mathbf{k}}} \; . \qquad (29)$$

For $V \simeq U$, $\Gamma_{03}^0 < 0$ so, since the sum over $\mathbf{k}$ is positive, $M_{\mathrm{HF}} > M$, as anticipated.

In short notations, and after analytic continuation on the real axis from above, $i\omega \to \omega + i\eta$, with $\eta > 0$ infinitesimal, the physical response functions are obtained through the set of linear equations:

$$\hat{\chi}(\omega, \mathbf{q}) = [\mathbb{1} - \hat{\chi}^{(0)}(\omega, \mathbf{q}) \, \hat{\Gamma}^0]^{-1} \, \hat{\chi}^{(0)}(\omega, \mathbf{q}) \,. \qquad (30)$$

The excitons are in-gap solutions $\omega_i(\mathbf{q})$, i.e.,

$$\omega_i(\mathbf{q}) < \omega_{\min}(\mathbf{q}) \equiv \min_{\mathbf{k}}(\epsilon_c(\mathbf{k} + \mathbf{q}) - \epsilon_v(\mathbf{k})) \,, \qquad (31)$$

of the equation

$$\det[\mathbb{1} - \hat{\chi}^{(0)}(\omega_i(\mathbf{q}), \mathbf{q}) \, \hat{\Gamma}^0] = 0 \,, \qquad (32)$$

and have either a z component of the spin $S_z = 0$, if they appear in the channels with $\alpha, \beta = 0, 3$, or $S_z = \pm 1$ in the channels with $\alpha, \beta = 1, 2$. For $\omega \simeq \omega_i(\mathbf{q})$, the response functions can be expanded in Laurent series [26],

$$\hat{\chi}(\mathbf{q}, \omega) = \sum_i \frac{A_i(\mathbf{q})}{\omega - \omega_i(\mathbf{q}) + i\eta} |\psi_i(\mathbf{q})\rangle \langle\psi_i(\mathbf{q})| + \dots, \quad (33)$$

where $|\psi_i(\mathbf{q})\rangle$ is the exciton wave function and $A_i(\mathbf{q})$ its spectral weight. This allows for computing the exciton Chern number through the integral of the Berry curvature:

$$C_i = \frac{1}{2\pi} \int d^2\mathbf{q} \; \Omega_i(\mathbf{q}) \,,$$
$$\Omega_i(\mathbf{q}) = \mathrm{Im} \, \langle\partial_x \psi_i(\mathbf{q}) \mid \partial_y \psi_i(\mathbf{q})\rangle \,. \qquad (34)$$

The curvature is even under inversion and odd under time reversal; if a system is invariant under both, the Chern number thus vanishes by symmetry.

We observe that all the excitons are invariant under inversion but, while the $S_z = 0$ ones are also invariant under time reversal, the latter maps the $S_z = +1$ and $S_z = -1$ excitons onto each other. Accordingly, only the $S_z = \pm 1$ excitons can have nonzero Chern numbers, actually opposite for opposite S_z, while the $S_z = 0$ excitons are constrained to have trivial topology. We stress that such a result, being based only upon symmetry considerations, remains valid for every inversion-symmetric QSHI, and not only in the context of the interacting BHZ model.

The exciton Chern number does not seem to be directly related to any quantized observable. Nonetheless, as pointed out in Refs. [26,38], a nonzero C_i ensures the presence of chiral exciton modes localized at the edges of the sample, which may have direct experimental consequences.
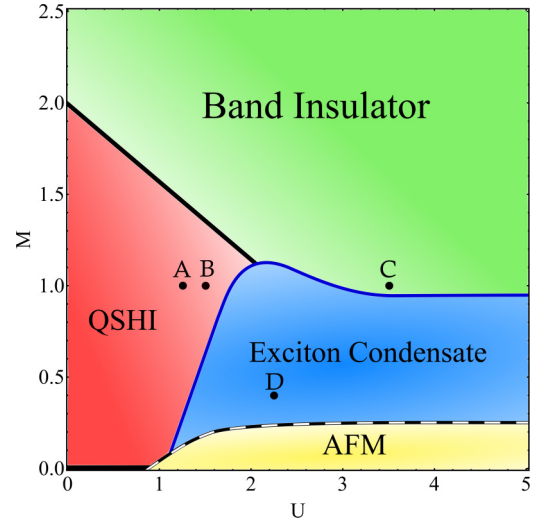

FIG. 2. Hartree-Fock phase diagram at $\lambda = 0.3$, $t' = 0.5$, $U_s = U_p = V = U$, and $J = U/16$. The topological insulator is denoted as QSHI, with the nontopological one as band insulator. For small value of M, antiferromagnetism (AFM) is stabilized upon increasing U. For larger values of M, U stabilizes a symmetry broken phase with exciton condensate. The thick black line that separates the QSHI from the band insulator, as well as that at $M = 0$ extending from $U = 0$ to the AFM phase, indicate a gapless metallic phase. The transition between the exciton insulator and the QSHI or the band insulator is continuous, while the transition into the AFM insulator is first order.

V. RESULTS

In the preceding sections, we have introduced a conserving mean-field scheme to consistently calculate both the phase diagram and the linear response functions. Now, we move to present the numerical results obtained by that method at zero temperature and with Hamiltonian parameters $t' = 0.5$, $\lambda = 0.3$, $V = U = U_s = U_p$, and $J = U/16$, see Eqs. (4), (13), (14), and (15). The value of J is estimated from $1s$ and $2p$ hydrogenoic orbitals, which may provide a reasonable estimate of the relative order of magnitude between the dipole interaction and the monopole one.

A. Hartree-Fock phase diagram

The HF phase diagram is shown in Fig. 2. As we previously mentioned, the interaction effectively increases M, thus pushing the transition from the topological insulator (QSHI) to the nontopological one (band insulator) to lower values of M the larger U. This is precisely what happens for $M \gtrsim 1.1$: U increases the effective M_{HF}, see Eq. (29), until $M_{\mathrm{HF}} = 2$. At this point, the gap closes and, for still larger U, the QSHI turns into the trivial band insulator.

For very small $M \lesssim 0.2$, upon increasing U the QSHI gives in to an antiferromagnetic insulator (AFM), characterized by finite order parameters $\Delta_{30}(\mathbf{R}_i) = \Delta_{30} e^{i\mathbf{Q}\cdot\mathbf{R}_i}$, see Eq. (21), with $\mathbf{Q} = (\pi, \pi)$, thus magnetized along z. HF predicts such a transition to be of first order, in accordance to more accurate dynamical mean-field theory calculations [39], which also explains why we do not find any precursory softening of $S_z = 0$ exciton at $\mathbf{Q}$.
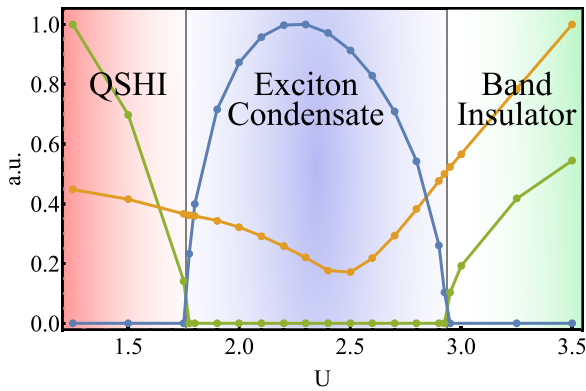
FIG. 3. Order parameter Δ of Eqs. (23) (blue), lowest $S_z = \pm 1$ exciton energy at $\mathbf{Q} = \mathbf{0}$ (green), and band gap (orange) along path A to C in Fig. 2 ($M = 1$, $U \in [1.25, 3.5]$), i.e., from the topological to the trivial insulator crossing the exciton insulator. We note that the intermediate phase emerges exactly when the exciton becomes massless, as well as that the band gap never vanishes.
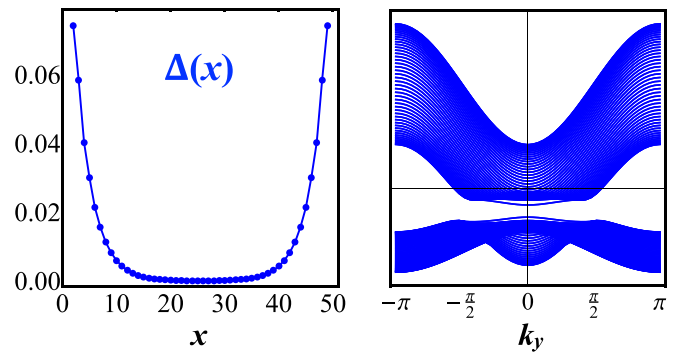

FIG. 4. Left panel: Exciton condensation order parameter $\Delta(x)$ in Eqs. (23) as function of the x coordinate in a ribbon geometry with $N_x = 50$ sites, calculated at point B in Fig. 2 ($M = 1$, $U = 1.5$). Right panel: The ribbon band structure as function of the momentum k_y. We note that, even though the condensate is exponentially localized at the edges of the system, still it has a strong effect on the single-particle edge states: A gap opens between the two branches, preventing topological spin transport.

More interesting is what happens for $0.2 \lesssim M \lesssim 1.1$. Here, increasing the interaction U drives a transition into a phase characterized by the finite order parameter in Eqs. (23), thus by a spontaneous symmetry breaking of spin $U(1)$, time reversal, and inversion symmetry. The breaking of time reversal allows the system to move from the QSHI to the band insulator without any gap closing [30–32], see Fig. 3. We note that the transition into the symmetry-variant phase happens to be continuous, at least within HF. As we mentioned, consistency of our approach implies that this transition must be accompanied by the softening of the excitons whose condensation signals the birth of the symmetry breaking. These excitons are those with $S_z = \pm 1$, and indeed get massless on both sides of the transition, see Fig. 3.

The HF numerical results in the ribbon geometry with OBC along x show that electron correlations get effectively enhanced near the boundaries [33–35], unsurprisingly because of the reduced coordination [40]. Indeed, the order parameter is rather large at the edges, and, moving away from them, decays exponentially toward its bulk value, as expected in an insulator. Remarkably, even when the bulk is in the QSHI stability region, a finite symmetry-breaking order parameter exponentially localized at the surface layer may still develop, see Fig. 4 that refers to point B in the phase diagram of Fig. 2. In the specific two-dimensional BHZ model that we study, such phenomenon is an artifact of the HF approximation, since the spin $U(1)$ symmetry cannot be broken along the one-dimensional edges. Nonetheless, the enhanced quantum fluctuations, while preventing a genuine symmetry breaking, should all the same substantially affect the physics at the edges.

We end the discussion of the HF phase diagram by comparing our results with those obtained by Xue and MacDonald [32]. These authors, too, apply the HF approximation to study the BHZ model but in the continuum limit and in the presence of a long-range Coulomb interaction. They also find a path between the topological insulator and the trivial one that crosses another insulating phase characterized by spontaneous time-reversal symmetry breaking, which, they argue, further

breaks C_4 symmetry, thus being nematic. The HF band structure that we find in the exciton condensate phase is instead perfectly C_4 invariant, which apparently might indicate that our phase and that of Ref. [32] are different. In reality, we believe the two phases are just the same phase. Indeed, while it is true that the order parameter Eqs. (23) is not invariant under the C_4 symmetry of Eq. (11) that changes $\phi \to \phi - \pi/2$, such a shift can be reabsorbed by a $-90°$ spin $U(1)$ rotation. In other words, the order parameter Eqs. (23) is invariant under a magnetic C_4' symmetry of the Hamiltonian, whose generator of $\pi/2$ rotations is $L_3 - S_3$ times the rotation of $\mathbf{k}$. Due to such residual symmetry, the band structure does not show nematicity, as well as the magnetoelectric tensor we shall discuss later in Sec. V C.

B. Excitons and their topological properties

The mechanism that triggers exciton topology is similar to the band inversion in the single-particle case: a topological exciton is composed by particle-hole excitations that have different parities under inversion in different regions of the BZ. In our case study, four possible orbital channels τ_a, $a = 0, \ldots, 3$, are allowed, each possessing a well-defined parity: τ_1 and τ_2 odd, while τ_0 and τ_3 even. In the nontopological insulator, the $S_z = \pm 1$ excitons have the same parity character at all inversion-invariant $\mathbf{k}$ points, $\mathbf{\Gamma}$, $\mathbf{M}$, $\mathbf{X}$, and $\mathbf{Y}$, and thus are topologically trivial. On the contrary, in the QSHI, the highly mixed bands entail that all channels have finite weight in the exciton, which may acquire nontrivial topology when its symmetry under parity changes among the inversion-invariant $\mathbf{k}$ points, thus entailing one or more avoided crossings.

In Fig. 5, we show the Chern number of the lowest energy exciton branch with $S_z = -1$ calculated through Eq. (34) with $U_s = U_p = V = 1.5$ as a function of M and J along the way from the QSHI to the symmetry-broken phase where excitons condense. We observe that the dipole-dipole interaction J favors not only the instability of the $S_z = \pm 1$ excitons, but also their nontrivial topology, signaled by a nonzero Chern
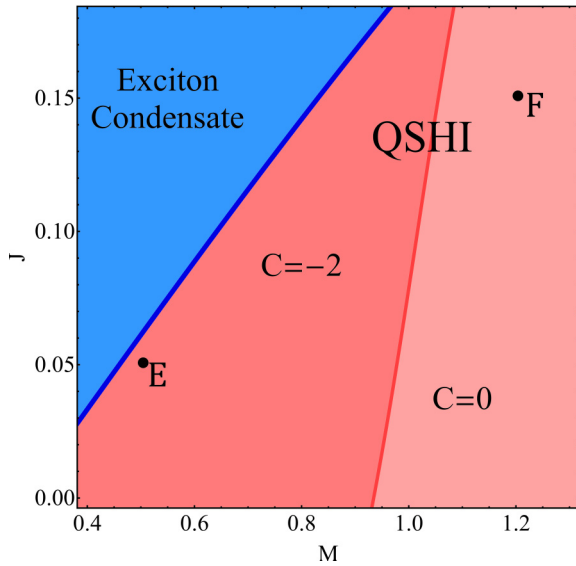
FIG. 5. Chern number of the most bound exciton with $S_z = -1$ at $\lambda = 0.3$, $t' = 0.5$, $U_s = U_p = V = 1.5$, as function of M and J close to the transition from the QSHI to the symmetry-broken phase.
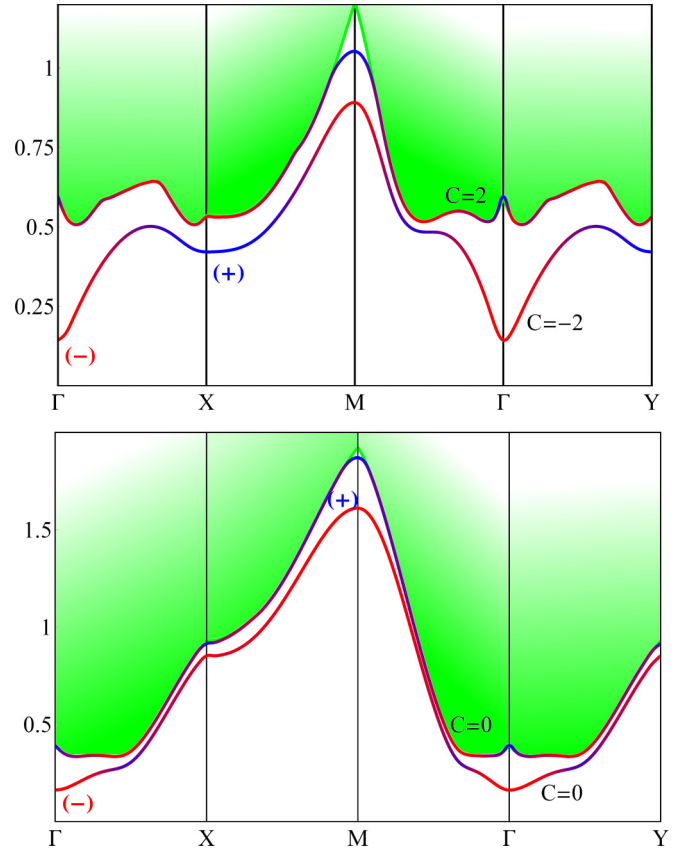

FIG. 6. $S_z = -1$ exciton dispersion along high-symmetry paths in the Brillouin zone, calculated for the two points E, top panel, and F, bottom panel, in Fig. 5. The green shaded regions are the particle-hole continuum. The blue and red colors of the curves indicate even $(+)$ and odd $(-)$ parity under inversion, while C is the corresponding Chern number.

number. In Fig. 6, we show for the two points E and F in Fig. 5 the $S_z = -1$ exciton bands, $\omega_i(\mathbf{q})$, $i = 1, 2$ along high-symmetry paths in the BZ, together with the continuum of $S_z = -1$ particle-hole excitations, bounded from below by $\omega_{\min}(\mathbf{q})$, see Eq. (31). The upper branch is very lightly bound and almost touches the continuum, unlike the lower branch, whose binding energy is maximum at the $\mathbf{\Gamma}$ point where, eventually, the condensation will take place. The blue and red colors indicate, respectively, even $(+)$ and odd $(-)$ parity character under inversion. We note that at point F in Fig. 5, both exciton bands have a vanishing Chern number, signaled by the same parity character at all inversion-invariant $\mathbf{k}$ points. On the contrary, at point E, close to the transition, the two exciton branches change parity character among the high-symmetry points, and thus acquire finite and opposite Chern numbers, $C = \pm 2$. For completeness, in Fig. 7 we show at the same points E and F of Fig. 5 the dispersion of the $S_z = 0$ excitons. Since they are invariant under time reversal, we also indicate their symmetry, even (black dots) or odd (yellow dots), which correspond, respectively, to the spin singlet and spin triplet with $S_z = 0$ components of the exciton.

Comparing Fig. 7 with 6, we note that the $S_z = 0$ excitons are far less bound than the $S_z = -1$ ones. However, it is conceivable that the inclusion of the long-range part of the Coulomb interaction could increase the binding energy of the $S_z = 0$ excitons, even though we believe that the $S_z = \pm 1$ excitons will still be lower in energy.

Moving to the sample surface at point E, we expect two phenomena to occur. First, chiral exciton edge modes should appear and connect the two branches with opposite Chern numbers, in analogy with the single-particle case, and as thoroughly discussed by the authors of Ref. [26] in the magnetized BHZ model. In addition, our previous results in the ribbon geometry, showing that the exciton condensate appears on the surface earlier than the bulk, suggest the existence of genuine

surface excitons, more bound than their bulk counterparts, definitely in the $S_z = \pm 1$ channel, but possibly also in the $S_z = 0$ one.

Both the chiral exciton edge modes as well as the surface excitons may potentially have important effects on the physical behavior at the boundaries. First, since the most bound ones correspond to coherent $S_z = \pm 1$ particle-hole excitations, they may provide efficient decay channels for the single-particle edge modes, which are counterpropagating waves with opposite $S_z = \pm 1/2$. Experimental evidence of such phenomenon in the purported topological Kondo insulator SmB$_6$ has indeed been observed [5,23] and previously attributed to scattering off bulk excitons [22]. This is very possible, but should be much less efficient than the scattering off surface exciton modes, which we propose as an alternative explanation. Furthermore, the presence of odd-parity excitons localized at the surface might have direct consequences on the surface optical activity, which could be worth investigating.

C. Exciton condensate and magnetoelectricity

Since the order parameter in the phase with exciton condensation breaks spin $U(1)$ symmetry, inversion $\mathcal{I}$, and time
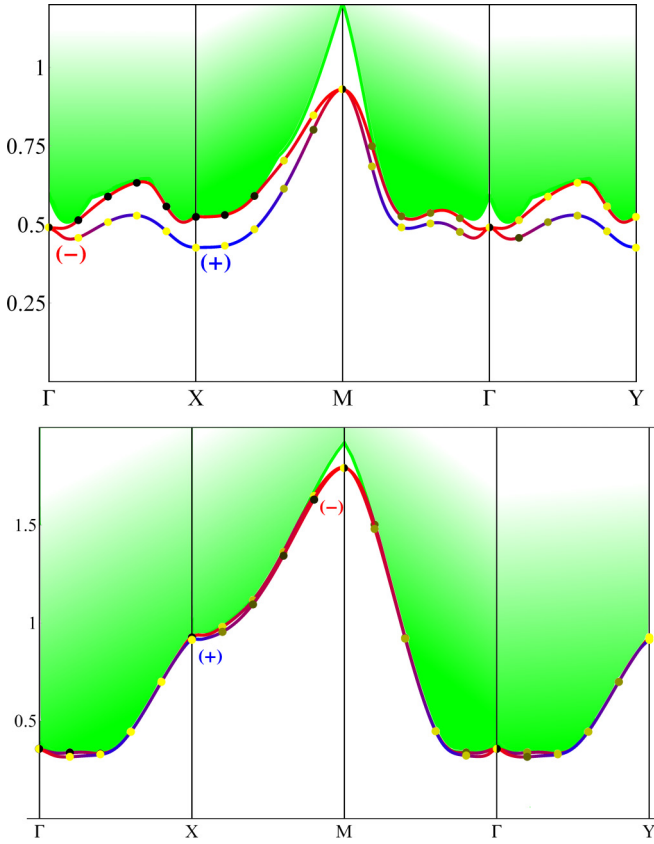
FIG. 7. Same as Fig. 6 but for the $S_z = 0$ excitons. Black and yellow dots indicate that the excitons are, respectively, even and odd under time reversal.

reversal $\mathcal{T}$, but not $\mathcal{T} \times \mathcal{I}$, it is eligible to display magneto-electric effects, which can be experimentally detected.

The free energy density expanded up to second order in the external electric and magnetic fields, both assumed constant in space and time, can be written as

$$F(\mathbf{E}, \mathbf{B}) = F_0 - \frac{1}{2} \boldsymbol{E} \cdot \hat{\chi}_e \, \boldsymbol{E} - \frac{1}{2} \boldsymbol{B} \cdot \hat{\chi} \, \boldsymbol{B} - \boldsymbol{E} \cdot \hat{\alpha} \, \boldsymbol{B}, \quad (35)$$

where $\hat{\chi}_e$, $\hat{\chi}$, and $\hat{\alpha}$ are the electric polarisability, magnetic susceptibility, and magnetoelectric tensors, respectively. The magnetization, $\boldsymbol{M}$, and polarization, $\boldsymbol{P}$, are conjugate variables of the fields, namely,

$$\boldsymbol{M} = -\frac{\partial F}{\partial \boldsymbol{B}} = \hat{\chi} \, \boldsymbol{B} + \hat{\alpha} \, \boldsymbol{E},$$

$$\boldsymbol{P} = -\frac{\partial F}{\partial \boldsymbol{E}} = \hat{\chi}_e \, \boldsymbol{E} + \hat{\alpha} \, \boldsymbol{B}. \quad (36)$$

We observe that, since $\boldsymbol{E}$ and $\boldsymbol{B}$ have opposite properties under inversion and time reversal, a nonzero $\hat{\alpha}$ is allowed only when both symmetries are broken, but not their product.

Since the exciton condensate Eqs. (23) is spin-polarized in the $x-y$ plane, with azimuthal angle ϕ, and involves dipole excitations $s \leftrightarrow p_{\pm 1}$, see Eqs. (1), we restrict our analysis to fields $\boldsymbol{E}$ and $\boldsymbol{B}$ that have only x and y components, which allows us to discard the electromagnetic coupling to the electron charge current. Consequently, the magnetoelectric tensor $\hat{\alpha}$ of our interest will be a 2×2 matrix with components α_{ij}, $i, j = x, y$.
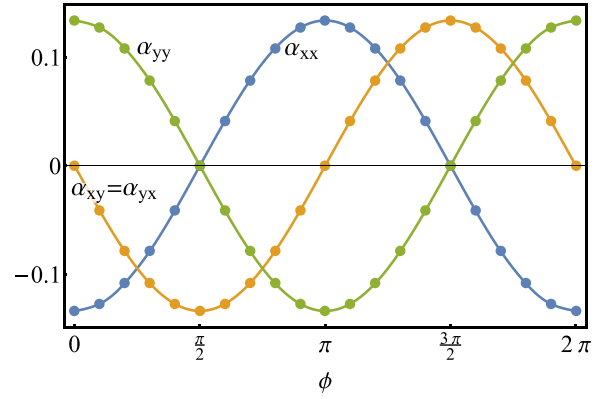

FIG. 8. Components of the magnetoelectric tensor $\hat{\alpha}$ calculated at point D in Fig. 2 ($M = 0.5, U = 2$). The data fit perfectly with the expression in Eq. (41).

In the exciton condensed phase, which is insulating, the coupling to the planar electric field is via the polarization density, namely, in proper units,

$$\delta H_E = -\sum_i \boldsymbol{\Psi}_i^\dagger \left(E_x \, \hat{d}_x + E_y \, \hat{d}_y \right) \boldsymbol{\Psi}_i, \quad (37)$$

with dipole operators

$$\hat{d}_x = \sigma_0 \otimes \tau_1, \quad \hat{d}_y = \sigma_3 \otimes \tau_2. \quad (38)$$

Moreover, as the orbitals $|s\,\sigma\rangle$ have physical total momentum $J_z = L_z + S_z = \pm 1/2$, while $|p\,\sigma\rangle$ have $J_z = \pm 3/2$, the in-plane magnetic field only couples to the magnetic moment of the s orbitals. Specifically,

$$\delta H_B = -\sum_i \boldsymbol{\Psi}_i^\dagger \left(B_x \, \hat{m}_x + B_y \, \hat{m}_y \right) \boldsymbol{\Psi}_i, \quad (39)$$

where

$$\hat{m}_x = \sigma_1 \otimes \frac{\tau_0 + \tau_3}{2}, \quad \hat{m}_y = \sigma_2 \otimes \frac{\tau_0 + \tau_3}{2}. \quad (40)$$

Since we are interested in the effects of the external fields once the symmetry has been broken, we performed a non-self-consistent calculation with the HF self-energy calculated at $\boldsymbol{E} = \boldsymbol{B} = 0$. The finite magnetoelectric effect in the presence of the exciton condensate is indeed confirmed, see Fig. 8 where we show the components of $\hat{\alpha}$ as function of the azimuthal angle ϕ in Eqs. (23), and which we find to behave as

$$\hat{\alpha} = \alpha_0 \begin{pmatrix} -\cos\phi & -\sin\phi \\ -\sin\phi & \cos\phi \end{pmatrix}, \quad (41)$$

where α_0 is proportional to the amplitude Δ of the order parameter, see Eqs. (23), and thus vanishes when the symmetry is restored.

We remark that the magnetoelectric tensor Eq. (41) has the form predicted for the magnetic point group $4'$ [41], thus not showing signals of the nematic order proposed in Ref. [32], as we earlier discussed in Sec. V A.

VI. CONCLUSIONS

In this paper, we have studied within a conserving mean-field scheme the role of a local electron repulsion in the

prototype BHZ model of a QSHI [28], whose symmetries allow, besides the conventional monopole components of Coulomb interaction, also a dipolar one, which we find to play a rather important role.

In the absence of interaction, the BHZ model displays, as a function of a mass parameter $M > 0$, two insulating phases, one topological at $M < M_c$, and another nontopological above M_c, separated by a metal point with Dirac-like dispersion at $M = M_c$. The primary effect of Coulomb interaction, namely, the level repulsion between occupied and unoccupied states, pushes the critical M_c to lower values, thus enlarging the stability region of the nontopological insulator. Besides that, and for intermediate values of M, our mean-field results predict that interaction makes a new insulating phase to intrude between the topological and nontopological insulators, uncovering a path connecting the latter two that does not cross any metal point. In this phase, inversion symmetry and time reversal are spontaneously broken, though their product is not, implying the existence of magnetoelectric effects. The approach to this phase from both topological and nontopological sides is signaled by the softening of two exciton branches, related to each other by time reversal and possessing, for $M \lesssim 1$ with the parameters of Fig. 2, finite and opposite Chern numbers. This phase can therefore be legitimately regarded as a condensate of topological excitons.

Since, starting from the QSHI, the softening of those excitons and their eventual condensation occurs upon increasing the interaction, it is rather natural to expect those phenomena to be enhanced at the surface layers. Indeed, the mean-field approach in a ribbon geometry predicts the surface instability to precede the bulk one. Even though a genuine exciton condensation at the surface layer might be prevented by quantum and thermal fluctuations, still it would sensibly affect the physics at the surface. The simplest consequence we may envisage is that the soft surface excitons would provide an efficient decay channel for the chiral single-particle edge modes, as indeed observed in the supposedly three-dimensional topological Kondo insulator SmB$_6$ [5,23]. In addition, we cannot exclude important consequences on the transport properties and optical activity at the surface.

We believe that going beyond the approximations assumed throughout this paper should not significantly alter our main results. Random phase approximation plus exchange allows accessing in a simple way collective excitations, though it ignores their mutual interaction. We expect that the latter would surely affect the precise location of the transition points, but not wash out the exciton condensation.

Inclusion of the neglected long-range tail of Coulomb interaction would introduce two terms: the standard monopole-monopole charge repulsion, proportional to $1/r$, and a dipole-dipole interaction decaying as $1/r^3$. The former is expected to increase the exciton binding energy, though without distinguishing between spin-singlet and -triplet channels. Therefore, our conclusion that the $S_z = \pm 1$ excitons soften earlier than the $S_z = 0$ ones should remain even in presence of the $1/r$ tail of Coulomb interaction. The dipole-dipole interaction might instead favor an inhomogeneous exciton condensation. However, we suspect that the $1/r^3$ decay in two dimensions is not sufficient to stablize domains. To conclude, we believe that our results, though obtained by a mean-field calculation and for a specific model topological insulator, catch sight of still not fully explored effects of electron-electron interaction in topological insulators, which might be worth investigating experimentally, as well as theoretically in other models and, eventually, by means of more reliable tools [42,43].

[1] B. Seradjeh, J. E. Moore, and M. Franz, Phys. Rev. Lett. **103**, 066402 (2009).

[2] D. I. Pikulin and T. Hyart, Phys. Rev. Lett. **112**, 176403 (2014).

[3] J. C. Budich, B. Trauzettel, and P. Michetti, Phys. Rev. Lett. **112**, 146405 (2014).

[4] W. T. Fuhrman, J. Leiner, P. Nikolić, G. E. Granroth, M. B. Stone, M. D. Lumsden, L. DeBeer-Schmitt, P. A. Alekseev, J.-M. Mignot, S. M. Koohpayeh et al., Phys. Rev. Lett. **114**, 036401 (2015).

[5] W. K. Park, L. Sun, A. Noddings, D.-J. Kim, Z. Fisk, and L. H. Greene, Proc. Natl. Acad. Sci. **113**, 6599 (2016).

[6] J. Knolle and N. R. Cooper, Phys. Rev. Lett. **118**, 096604 (2017).

[7] L. Du, X. Li, W. Lou, G. Sullivan, K. Chang, J. Kono, and R.-R. Du, Nat. Commun. **8**, 1971 (2017).

[8] S. Kung, A. Goyal, D. Maslov, X. Wang, A. Lee, A. Kemper, S.-W. Cheong, and G. Blumberg, Proc. Natl. Acad. Sci. **116**, 4006 (2019).

[9] D. Varsano, M. Palummo, E. Molinari, and M. Rontani, Nat. Nanotechnol. **15**, 367 (2020).

[10] X. Qian, J. Liu, L. Fu, and J. Li, Science **346**, 1344 (2014).

[11] S. Tang, C. Zhang, D. Wong, Z. Pedramrazi, H.-Z. Tsai, C. Jia, B. Moritz, M. Claassen, H. Ryu, S. Kahn et al., Nat. Phys. **13**, 683 (2017).

[12] L. Peng, Y. Yuan, G. Li, X. Yang, J.-J. Xian, C.-J. Yi, Y.-G. Shi, and Y.-S. Fu, Nat. Commun. **8**, 659 (2017).

[13] D. K. Efimkin, Y. E. Lozovik, and A. A. Sokolik, Phys. Rev. B **86**, 115436 (2012).

[14] D. J. J. Marchand and M. Franz, Phys. Rev. B **86**, 155146 (2012).

[15] M. P. Mink, H. T. C. Stoof, R. A. Duine, M. Polini, and G. Vignale, Phys. Rev. Lett. **108**, 186402 (2012).

[16] Y. E. Lozovik and A. A. Sokolik, JETP Lett. **87**, 55 (2008).

[17] H. Min, R. Bistritzer, J.-J. Su, and A. H. MacDonald, Phys. Rev. B **78**, 121401(R) (2008).

[18] X. Liu, K. Watanabe, T. Taniguchi, B. I. Halperin, and P. Kim, Nat. Phys. **13**, 746 (2017).

[19] N. J. Laurita, C. M. Morris, S. M. Koohpayeh, P. F. S. Rosa, W. A. Phelan, Z. Fisk, T. M. McQueen, and N. P. Armitage, Phys. Rev. B **94**, 165154 (2016).

[20] J. Stankiewicz, M. Evangelisti, P. F. S. Rosa, P. Schlottmann, and Z. Fisk, Phys. Rev. B **99**, 045138 (2019).

[21] M. Hartstein, W. H. Toews, Y. T. Hsu, B. Zeng, X. Chen, M. C. Hatnean, Q. R. Zhang, S. Nakamura, A. S. Padgett, G. Rodway-Gant *et al.*, Nat. Phys. **14**, 166 (2018).

[22] G. A. Kapilevich, P. S. Riseborough, A. X. Gray, M. Gulacsi, T. Durakiewicz, and J. L. Smith, Phys. Rev. B **92**, 085133 (2015).

[23] A. Arab, A. X. Gray, S. Nemšák, D. V. Evtushinsky, C. M. Schneider, D.-J. Kim, Z. Fisk, P. F. S. Rosa, T. Durakiewicz, and P. S. Riseborough, Phys. Rev. B **94**, 235125 (2016).

[24] K. Akintola, A. Pal, S. R. Dunsiger, A. C. Y. Fang, M. Potma, S. R. Saha, X. Wang, J. Paglione, and J. E. Sonier, njp Quantum Mater. **3**, 36 (2018).

[25] I. Garate and M. Franz, Phys. Rev. B **84**, 045403 (2011).

[26] K. Chen and R. Shindou, Phys. Rev. B **96**, 161101(R) (2017).

[27] A. A. Allocca, D. K. Efimkin, and V. M. Galitski, Phys. Rev. B **98**, 045430 (2018).

[28] B. A. Bernevig, T. L. Hughes, and S.-C. Zhang, Science **314**, 1757 (2006).

[29] M. Altmeyer, D. Guterding, P. J. Hirschfeld, T. A. Maier, R. Valentí, and D. J. Scalapino, Phys. Rev. B **94**, 214515 (2016).

[30] T. L. Hughes, E. Prodan, and B. A. Bernevig, Phys. Rev. B **83**, 245132 (2011).

[31] M. Ezawa, Y. Tanaka, and N. Nagaosa, Sci. Rep. **3**, 2790 (2013).

[32] F. Xue and A. H. MacDonald, Phys. Rev. Lett. **120**, 186802 (2018).

[33] A. Shitade, H. Katsura, J. Kuneš, X.-L. Qi, S.-C. Zhang, and N. Nagaosa, Phys. Rev. Lett. **102**, 256403 (2009).

[34] A. Medhi, V. B. Shenoy, and H. R. Krishnamurthy, Phys. Rev. B **85**, 235449 (2012).

[35] A. Amaricci, L. Privitera, F. Petocchi, M. Capone, G. Sangiovanni, and B. Trauzettel, Phys. Rev. B **95**, 205120 (2017).

[36] D. G. Rothe, R. W. Reinthaler, C.-X. Liu, L. W. Molenkamp, S.-C. Zhang, and E. M. Hankiewicz, New J. Phys. **12**, 065012 (2010).

[37] C. L. Kane and E. J. Mele, Phys. Rev. Lett. **95**, 226801 (2005).

[38] R. S. K. Mong and V. Shivamoggi, Phys. Rev. B **83**, 125109 (2011).

[39] A. Amaricci, A. Valli, G. Sangiovanni, B. Trauzettel, and M. Capone, Phys. Rev. B **98**, 045133 (2018).

[40] G. Borghi, M. Fabrizio, and E. Tosatti, Phys. Rev. Lett. **102**, 066806 (2009).

[41] J. P. Rivera, Eur. Phys. J. B **71**, 299 (2009).

[42] A. Amaricci, J. C. Budich, M. Capone, B. Trauzettel, and G. Sangiovanni, Phys. Rev. Lett. **114**, 185701 (2015).

[43] A. Amaricci, J. C. Budich, M. Capone, B. Trauzettel, and G. Sangiovanni, Phys. Rev. B **93**, 235112 (2016).